Adv. Manuf. (2020) 8:486–507
https://doi.org/10.1007/s40436-020-00326-x

Prediction and control of surface roughness for the milling of Al/SiC metal matrix composites based on neural networks

Guo Zhou[1] · Chao Xu[2,3] · Yuan Ma[2,3] · Xiao-Hao Wang[1,2] · Ping-Fa Feng[2,3] · Min Zhang[2]

Received: 17 February 2020 / Revised: 8 May 2020 / Accepted: 13 October 2020 / Published online: 23 November 2020

Abstract In recent years, there has been a significant increase in the utilization of Al/SiC particulate composite materials in engineering fields, and the demand for accurate machining of such composite materials has grown accordingly. In this paper, a feed-forward multi-layered artificial neural network (ANN) roughness prediction model, using the Levenberg-Marquardt backpropagation training algorithm, is proposed to investigate the mathematical relationship between cutting parameters and average surface roughness during milling Al/SiC particulate composite materials. Milling experiments were conducted on a computer numerical control (CNC) milling machine with polycrystalline diamond (PCD) tools to acquire data for training the ANN roughness prediction model. Four cutting parameters were considered in these experiments: cutting speed, depth of cut, feed rate, and volume fraction of SiC. These parameters were also used as inputs for the ANN roughness prediction model. The output of the model was the average surface roughness of the machined workpiece. A successfully trained ANN roughness prediction model could predict the corresponding average surface roughness based on given cutting parameters, with a 2.08% mean relative error. Moreover, a roughness control model that could accurately determine the corresponding cutting parameters for a specific desired roughness with a 2.91% mean relative error was developed based on the ANN roughness prediction model. Finally, a more reliable and readable analysis of the influence of each parameter on roughness or the interaction between different parameters was conducted with the help of the ANN prediction model.

Keywords Al/SiC metal matrix composite (MMC) · Surface roughness · Prediction · Control · Neural network

List of symbols

ANN	Artificial neural network
CNC	Computer numerical control
PCD	Polycrystalline diamond
MMC	Metal matrix composite
V_c	Cutting speed
F_r	Feed rate
D_c	Depth of cut
φ_{SiC}	Volume fraction of SiC
o_m^k	Output of the mth neuron in the layer under consideration
o_n^{k-1}	Output of the nth neuron in the preceding layer
w_{mn}	Weight value of the connection between the mth neuron in the layer under consideration and the nth neuron in the preceding layer
b_m^k	Bias value for the mth neuron in the layer under consideration
$f_{activation}$	Activation function
$R_{a\_predicted}$	Output roughness value by the prediction model
R_{a_target}	Real roughness value of the milled surface
E_i	Error between $R_{a\_predicted\_i}$ and $R_{a\_target\_i}$ for the ith input vector

✉ Min Zhang
zhang.min@sz.tsinghua.edu.cn

[1] Tsinghua-Berkeley Shenzhen Institute, Tsinghua University, Shenzhen 518055, Guangdong, People's Republic of China

[2] Shenzhen International Graduate School, Tsinghua University, Shenzhen 518055, Guangdong, People's Republic of China

[3] Department of Mechanical Engineering, Tsinghua University, Beijing 100084, People's Republic of China

S_i	Squared error between $R_{a\_predicted\_i}$ and $R_{a\_target\_i}$ for the ith input vector
$\boldsymbol{W}_{bnew}$	New weights-bias matrix which consists of all weights and biases updated over $\boldsymbol{W}_{bold}$ after the ith input vector used for training
$\boldsymbol{W}_{bold}$	Old weights-bias matrix which consists of all weights and biases
$\boldsymbol{J}$	Jacobian matrix
P	Number of elements in weights-bias matrix
$\boldsymbol{I}$	Unit matrix
μ	Adaptive factor
P_{model}	Roughness prediction model
E_t	Tolerable error
ANOVA	Analysis of variance
BUE	Built-up edge

1 Introduction

In recent decades, metal matrix composite (MMC) materials have been widely used in engineering fields due to their superior mechanical and physical properties, such as specific strength, high stiffness, and wear resistance. Aluminum reinforced with SiC particulates is a typical MMC material and has replaced conventional materials in the automotive, aerospace, and other diverse industries [1–4]. This material can provide higher strength, stiffness, and fatigue resistance compared to the base alloy, with only a small increase in density [5, 6]. These superior properties contribute to the broader application of Al/SiC composite materials. However, low plasticity, non-uniformity, and uncontrollable distribution of SiC particulate increase the difficulty of achieving a high surface quality when machining Al/SiC composite materials. Despite the sophisticated manufacturing techniques for producing satisfactory Al/SiC MMC components, e.g., via near-net shaping and casting processes, a high-quality machining process is still essential to meet the requirements of high surface quality and dimensional accuracy [7].

Over the past two decades, the issues of machining MMC materials have been investigated by researchers from both academia and industry. It is accepted that the morphology, distribution, and volume fraction of the reinforcement particulate in MMC materials are significant factors in affecting the cutting process, compared with conventional materials [8]. The effects of spindle speed, feed rate, depth of cut, rake angle, coolant on the cutting forces, tool wear, and surface quality were studied by Hoecheng et al. [9]. Chan et al. [10] also investigated the influence of cutting parameters on surface quality in ultra-precision diamond machining of Al/SiC/15P. They concluded that a high spindle speed and low feed rate could improve the surface quality but the effect of cutting depth on surface quality was small, dependent on the spindle speed not being too low. Pramanik et al. [11] conducted experiments on machining Al6061/SiC/15P materials and found that surface quality was mainly affected by feed rate, while the influence of spindle speed was negligible. Manna and Bhattacharyya [12] researched the relationship between parametric combination and surface finish during turning of Al/SiC-MMC via analysis of variance (ANOVA) and Taguchi experiment design and proposed that cutting speed, feed rate, and depth of cut had approximately equal influence on the average surface roughness. Similarly, Palanikumar and Karthikeyan [13] used ANOVA to analyze the influence of cutting factors (cutting speed, feed rate, depth of cut, and volume fraction of SiC) on surface roughness when machining Al/Si composites and proved that the feed rate had the greatest influence on surface roughness, followed by cutting speed and volume fraction of SiC. Przestacki et al. [14] determined that selection of the effective depth of cut and the tool's angular distance from the laser beam affected the machined surface quality during laser-assisted turning of A359/20SiCP MMCs. Wojciechowski et al. [15] proposed that surface roughness during the machining of direct laser deposited tungsten was influenced by kinematic-geometric factors and elastic-plastic phenomena that occurred when the uncut chip thickness was shallow. Kilickap [16] investigated the influences of cutting speed, feed rate, heat treatment, and cutting environment on surface roughness during drilling of Al/SiC MMC and found introducing the MQL technique improved surface quality. Kilickap et al. [17] also selected homogenized 5% SiC-p aluminum MMC material experimental investigation of tool wear and surface roughness. The authors found that tool wear was mainly affected by cutting speed and increased with increasing cutting speed during dry turning conditions.

The literature mentioned above predominantly studied the influence of different parameters on surface quality during machining Al/SiC composites; they provided a qualitative rather than quantitative relationship between parameters and surface roughness. Regarding the prediction and control of machining quality via machine learning methods, there has been some research on materials other than Si/Al composites and investigation of characteristics other than machining quality. Moreover, the performance and comparison of different machine learning methods used in machining fields was further investigated by various researchers. Benardros and Vosniakos [18] used an artificial neural network (ANN) method to predict surface roughness based on depth of cut, feed rate, cutting speed, engagement of tool, cutting tool type, and use of coolant when machining alloy using the Taguchi design of experiments method. The mean squared error of validating this

ANN model was 1.86%. Mahesh et al. [19] used a genetic algorithm to predict surface roughness in terms of cutting speed, feed rate, axial depth of cut, radial depth of cut, and radial rake angle for end milling 6063Al. However, experimental data were limited, which might have influenced the reliability of the prediction model. Kilickap et al. [20] used genetic algorithms for optimizing machining conditions to minimize surface roughness when drilling AISI 1045. The minimum surface roughness (R_a = 1.89 μm) value was obtained at V = 7.62 m/min, f = 0.1 mm/r, and MQL. An ANN model was suggested by Khorasani et al. [21] to predict the tool life based on cutting speed, depth of cut, and feed rate when face milling machining of 7075 Al with a 4.6% mean relative error. Pimenov et al. [22] investigated the effects of the relative position of the face mill with respect to the workpiece and milling kinematics on the cutting forces, vibration acceleration, and surface roughness during face milling, with the help of an artificial intelligence model. Bustillo and Correa [23] applied Bayesian networks to predict surface roughness when deep drilling steel components. Rodríguez et al. [24] predicted the roughness for face milling 11SMnPb37 steel in terms of tool wear and type, using the decision tree method. A fuzzy logic model was employed by Çelik et al. [25] to estimate the surface roughness and thrust force based on different cutting parameters during end milling of GFRPC materials; they found low feed rate, high cutting speed, and a large number of flutes resulted in low surface roughness. Lin et al. [26] studied the relationship between feed force and tool wear when machining A359 Al/SiC composites and found that using the ANN method to define this relationship was more accurate compared with regression analysis. Mia et al. [27] compared the performance of the teaching-learning-based optimization method and bacterial foraging optimization method by using these two methods to obtain the optimum cutting speed, feed rate, and depth of cut for the lowest surface roughness and cutting temperature during hard-turning hardened high-carbon steel; they determined that the first optimization method was recommended. Ensemble learning, which could avoid neural network fine-tuning, compared to a single learning algorithm, was used to build the roughness prediction model for ball-end milling by Bustillo et al. [28]. Kilickap et al. [29] used ANN and RSM models to predict cutting force, surface roughness, and tool wear based on cutting speed, feed rate, and depth of cut when milling Ti-6242S; they found that the accuracy of the ANN model was higher than that of the RSM model.

From the aforementioned Refs. [18–29], it could be seen that artificial intelligence methods were valid and reliable means of investigating the quantitative relationship between surface quality and cutting parameters (or other parameters). However, research regarding roughness prediction and control for machining Al/SiC composites is too limited; this is the primary motivation for our work. The purpose of this study is to develop a roughness prediction and control model for milling Al/SiC composite materials. With the help of the control model, apart manufactured from Al/SiC composite materials could be produced with any specific surface roughness. The utilization of such potential materials would be promoted accordingly. Moreover, this study analyzes the influence of cutting parameters on roughness, based on the roughness prediction model. Various exciting and novel findings were obtained, which might be of value as a reference for future researchers.

2 Experiment

2.1 Identification of cutting parameters and their levels

With regard to the above Refs. [8–17], factors that have a significant influence on surface roughness during milling Al/SiC MMC include the following: (i) spindle speed, (ii) feed rate, (iii) depth of cut, (iv) volume fraction of SiC, (v) cutting forces, (vi) vibration of machine, (vii) temperature, and (viii) tool character. Clearly, investigating the influence of all of these factors on surface roughness would significantly increase the intricacy of the experiment and was determined to be unnecessary. Moreover, the uncontrollable factors (v)–(vii) depend on factors (i)–(iv) and (viii), which are controllable. In our experiment, cutting parameter (viii) was defined as a constant to reduce the complexity and cost of the experiment. Therefore, cutting parameters (i)–(iv) were selected for study of their effect on surface roughness when machining Al/SiC MMC. To ensure the feasibility and safety of the experiments, the level values of these selected parameters were appropriately identified, subsequent to detailed analysis. The ranges of level values and reasons are explained in the following.

(i) Cutting speed. According to Ref. [30], excessively low speed results in poor surface roughness but excessively high speeds increases the temperature of the tool, accelerating tool wear. The max speed of the machine in our lab was 8 000 r/min and the diameter of the tool insert was just 6 mm; thus, the max cutting speed was approximately 150 m/min. Taking the surface quality, tool wear, and machine stability into consideration, the range of cutting speed was set as 40–100 m/min.

(ii) Feed rate. According to Refs. [31, 32], a high feed rate increases cutting force and accelerates tool wear when milling MMC materials. However, an

excessively low feed rate directly decreases machining efficiency. To balance efficiency and cost, the feed rate was set at 0.1–0.4 mm/r.

(iii) Depth of cut. High depth also increases cutting force. A test experiment was conducted and found there was abnormal noise occurring in the machine when the depth value was 0.2 mm. Conversely, excessive low depth dramatically decreases machining efficiency in practical production. The range of depth of cut was thus set at 0.05–0.15 mm.

(iv) Volume fraction of SiC. The existence of SiC particulates increased the difficulty of machining [31]. A large volume fraction of SiC would lead to extremely poor surface roughness; conversely, the influence of other parameters, such as cutting speed, feed rate, and depth of cut, on surface roughness would be weakened, which was undesirable for this study. The range of volume fraction of SiC was thus set at 0–30%.

2.2 Design of experiment matrix

The number of levels of each selected parameter was set as three and the values are shown in Table 1, based on the range of level values mentioned in the previous section. In this experiment, all possible combinations of levels were covered, i.e., there were 3^4 (3 was the number of levels and 4 was the number of parameters) trials in total. Other authors [18, 33–36] applied Taguchi experiment design to reduce the considerable number of trials. However, this method would damage the experimental data's integrity and consequently influence the reliability of the neural network model and accuracy of the data analysis. A large number of trials could be completed in a shorter space of time than anticipated when aided by the CNC machine programming system.

2.3 Selection of tool and materials and conduction of experiment

Al2009, Al2009/SiC/15P, and Al2009/SiC/25P MMCs, three materials with different volume fraction of SiC, were selected as workpiece materials in this experiment. The workpiece material was fabricated via the powder metallurgy method using Al2009 (Cu: 4.5% (mass fraction), Mg: 1.5% (mass fraction), Al: redundant) powder and SiC powder. The average grain size of the Al2009 and SiC powder was approximately 30 μm and 12 μm, respectively. The first fabrication step was to mix these two powders uniformly in a three-dimensional tubular mixer for 40 min. The second step was to cold compact the mixed powders at a pressure of 350 MPa. The sintering operation was then conducted at 550 °C for 1 h. Finally, the sample materials were extruded in a pre-heated mold at 500 °C. Al2009 is selected as the matrix as it is a comparatively new type of aluminum alloy with some unique characteristics; research on Al/SiC composites with Al2009 has been limited up until now. The workpiece of each material was a block with dimensions 50 mm × 50 mm × 20 mm. El-Gallab and Sklad [37] found that the PCD tool had a longer life than other tools. Therefore, a 2-tooth PCD tool was selected to machine the Al/SiC composites with high wear resistance in this experimentation. An emulsion was used as a coolant throughout this experiment. This experiment was conducted on a specific milling machine. The milling machine and PCD tool information can be seen in Fig. 1.

The face milling operations were performed as per the condition given by the design matrix randomly. Table 2 shows the experiment design matrix and corresponding measured average surface roughness. Average surface roughness has received most attention from the industry field and was thus taken as the object of this study. To obtain average roughness measurement, the roughness tester probe was moved 2.5 mm in the feed direction along the milled surface, gathering values at five different locations; the average of these values was then used. The deviation of the tester was 0.001 μm. All experimental data used for building the ANN model was shown in Table 2. According to Grzenda et al. [38], an incomplete or partly

Table 1 Settings of parameters' level values

No.	Parameter	Notation	Unit	Level		
				1	2	3
1	Cutting speed	V_c	m/min	40	70	100
2	Feed rate	F_r	mm/r	0.10	0.25	0.40
3	Depth of cut	D_c	mm	0.05	0.10	0.15
4	Volume fraction of SiC	φ_{SiC}	%	0	15	25

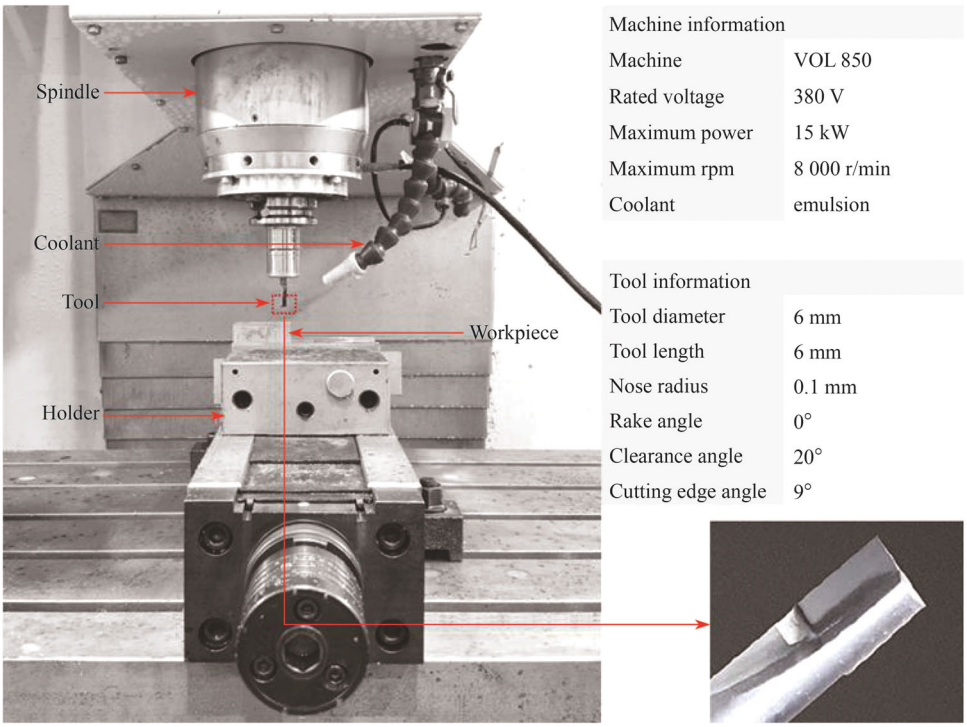

Machine information	
Machine	VOL 850
Rated voltage	380 V
Maximum power	15 kW
Maximum rpm	8 000 r/min
Coolant	emulsion

Tool information	
Tool diameter	6 mm
Tool length	6 mm
Nose radius	0.1 mm
Rake angle	0°
Clearance angle	20°
Cutting edge angle	9°

Fig. 1 Information of machine and tool

wrong dataset will lead to an unreliable roughness prediction model. Therefore, the imputation of missing data before the training process was a necessary and essential procedure. We repeatedly checked the completeness and correctness of our experimental data. We found that our data were reliable (the mean relative error of the validation of Model 1 in Table 3 was just 3.50%); therefore, the imputation of missing data step was omitted from this study.

3 Development of the roughness prediction and control model

3.1 Development of the roughness prediction model

With the further development of artificial intelligence and machine learning, their application has rapidly spread to the field of engineering. ANN has the powerful ability to learn complicated and non-linear relationships between multiple variables with high accuracy. Therefore, ANN was selected for studying the relationship between cutting parameters and surface roughness. In this section, a feed-forward multi-layered perceptron ANN roughness prediction model with a Levenberg-Marquardt backpropagation training algorithm was trained and validated using experimental data.

3.1.1 Structure of a multi-layered ANN model

The human brain is a classic biological neural network. The ANN has been developed to learn from pre-existing pure data to obtain deeper knowledge or determine patterns regarding this data, emulating the brain. Figure 2 shows the general structure of a multi-layered perceptron neural network, consisting of an input layer, one hidden layer, and an output layer. Each neuron from one layer was connected with all neurons from the neighboring layer so that the entire structure resembled a network. Functionally, the input layer input the data into the network without any processing. The complex data processing was conducted by the hidden layer and the output layer, as shown in Fig. 3. The training process of the neural network model involved iteratively adjusting the connection weight between neurons and the biases of the neurons until specific requirements were satisfied.

3.1.2 Procedure of building the ANN model

The following statements give the detailed steps of training the ANN model.

Step 1 Set parameters of the network model. The following statements describe these parameters and the setting rules.

(i) Number of hidden layers. There was no strict rule of selection regarding the number of

Table 2 Experiment design matrix and experiment data

No.	φ_{SiC}/%	V_c/(m·min^{-1})	F_r/(mm·r^{-1})	D_c/mm	R_a/μm	No.	φ_{SiC}/%	V_c/(m·min^{-1})	F_r/(mm·r^{-1})	D_c/mm	R_a/μm	No.	φ_{SiC}/%	V_c/(m·min^{-1})	F_r/(mm·r^{-1})	D_c/mm	R_a/μm
1	0	40	0.10	0.05	0.170	28	15	40	0.10	0.05	0.187	55	25	40	0.10	0.05	0.178
2	0	40	0.10	0.10	0.181	29	15	40	0.10	0.10	0.196	56	25	40	0.10	0.10	0.185
3	0	40	0.10	0.15	0.194	30	15	40	0.10	0.15	0.192	57	25	40	0.10	0.15	0.212
4	0	70	0.10	0.05	0.134	31	15	70	0.10	0.05	0.177	58	25	70	0.10	0.05	0.171
5	0	70	0.10	0.10	0.138	32	15	70	0.10	0.10	0.181	59	25	70	0.10	0.10	0.172
6	0	70	0.10	0.15	0.151	33	15	70	0.10	0.15	0.197	60	25	70	0.10	0.15	0.200
7	0	100	0.10	0.05	0.130	34	15	100	0.10	0.05	0.164	61	25	100	0.10	0.05	0.164
8	0	100	0.10	0.10	0.135	35	15	100	0.10	0.10	0.175	62	25	100	0.10	0.10	0.168
9	0	100	0.10	0.15	0.142	36	15	100	0.10	0.15	0.180	63	25	100	0.10	0.15	0.180
10	0	40	0.25	0.05	0.257	37	15	40	0.25	0.05	0.295	64	25	40	0.25	0.05	0.353
11	0	40	0.25	0.10	0.308	38	15	40	0.25	0.10	0.349	65	25	40	0.25	0.10	0.382
12	0	40	0.25	0.15	0.334	39	15	40	0.25	0.15	0.389	66	25	40	0.25	0.15	0.419
13	0	70	0.25	0.05	0.191	40	15	70	0.25	0.05	0.242	67	25	70	0.25	0.05	0.294
14	0	70	0.25	0.10	0.222	41	15	70	0.25	0.10	0.304	68	25	70	0.25	0.10	0.341
15	0	70	0.25	0.15	0.266	42	15	70	0.25	0.15	0.355	69	25	70	0.25	0.15	0.406
16	0	100	0.25	0.05	0.188	43	15	100	0.25	0.05	0.193	70	25	100	0.25	0.05	0.227
17	0	100	0.25	0.10	0.216	44	15	100	0.25	0.10	0.234	71	25	100	0.25	0.10	0.259
18	0	100	0.25	0.15	0.249	45	15	100	0.25	0.15	0.265	72	25	100	0.25	0.15	0.299
19	0	40	0.40	0.05	0.423	46	15	40	0.40	0.05	0.604	73	25	40	0.40	0.05	0.718
20	0	40	0.40	0.10	0.488	47	15	40	0.40	0.10	0.714	74	25	40	0.40	0.10	0.778
21	0	40	0.40	0.15	0.585	48	15	40	0.40	0.15	0.785	75	25	40	0.40	0.15	0.860
22	0	70	0.40	0.05	0.366	49	15	70	0.40	0.05	0.568	76	25	70	0.40	0.05	0.636
23	0	70	0.40	0.10	0.401	50	15	70	0.40	0.10	0.577	77	25	70	0.40	0.10	0.658
24	0	70	0.40	0.15	0.436	51	15	70	0.40	0.15	0.664	78	25	70	0.40	0.15	0.681
25	0	100	0.40	0.05	0.321	52	15	100	0.40	0.05	0.346	79	25	100	0.40	0.05	0.404
26	0	100	0.40	0.10	0.370	53	15	100	0.40	0.10	0.354	80	25	100	0.40	0.10	0.427
27	0	100	0.40	0.15	0.373	54	15	100	0.40	0.15	0.515	81	25	100	0.40	0.15	0.457

Table 3 Configurations and performances of different models

Model parameter	Model		
	1	2	3
Configurations			
Training algorithms	Levenberg-Marquardt backpropagation	Gradient descent backpropagation	Bayesian regulation backpropagation
Number of hidden layers	1	1	1
Number of neurons in input layer	4	4	4
Number of neurons in hidden layers	9	9	9
Number of neurons in output layer	1	1	1
Activation function for hidden layer(s)	SoftMax	SoftMax	SoftMax
Activation function for output layer	Pure linear	Pure linear	Pure linear
Learning rate	Adaptive	0.9	Adaptive
Tolerable error	0	0	0
Minimum MSE gradient	10^{-7}	10^{-5}	10^{-7}
Maximum iterations	1 000	10 000	1 000
Performance			
Iterations required for convergence	15	7137	126
Mean squared error of the validation	8.59×10^{-5}	1.40×10^{-3}	7.54×10^{-5}
Mean relative error of the validation/%	3.50	13.93	3.67

Note: The weights and biases for Models 1, 2 and 3 can be seen in the following pages

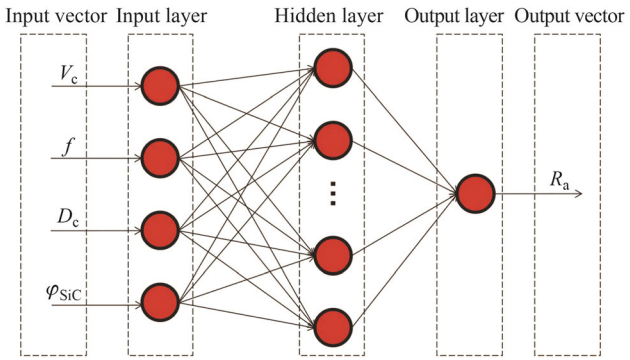

Fig. 2 Structure of multi-layered perceptron ANN

hidden layers [39]. However, the original number of hidden layers was generally set as one and then increased until the accuracy of the network model lay within an expected range of values, with a practical iteration count and cost of computing power.

(ii) Number of neurons in all layers. The number of neurons in the input and output layer was equal to the number of variables in the input vector and output layer, respectively. The number of neurons in the hidden layer was generally set as $2n + 1$ (n is the number of neurons in the input layer), based on the Kolmogorov theorem.

(iii) Activation function. For the regressor problems, to which the problem in this paper belonged, the sigmoid or SoftMax function was the most popular activation function set for hidden layers and the linear function was set as the activation function for the output layer.

(iv) Training algorithm. There are several popular training algorithms. The gradient descent backpropagation algorithm [40], which is the most common and easiest to use but struggles to converge when the training dataset is small; Levenberg-Marquardt backpropagation [41], which performs well for the majority of problems; and Bayesian regulation backpropagation [42], which contains some modifications to Levenberg-Marquardt backpropagation and is suitable for datasets containing noise but the convergence rate is lower. The size of data used for training in this study was

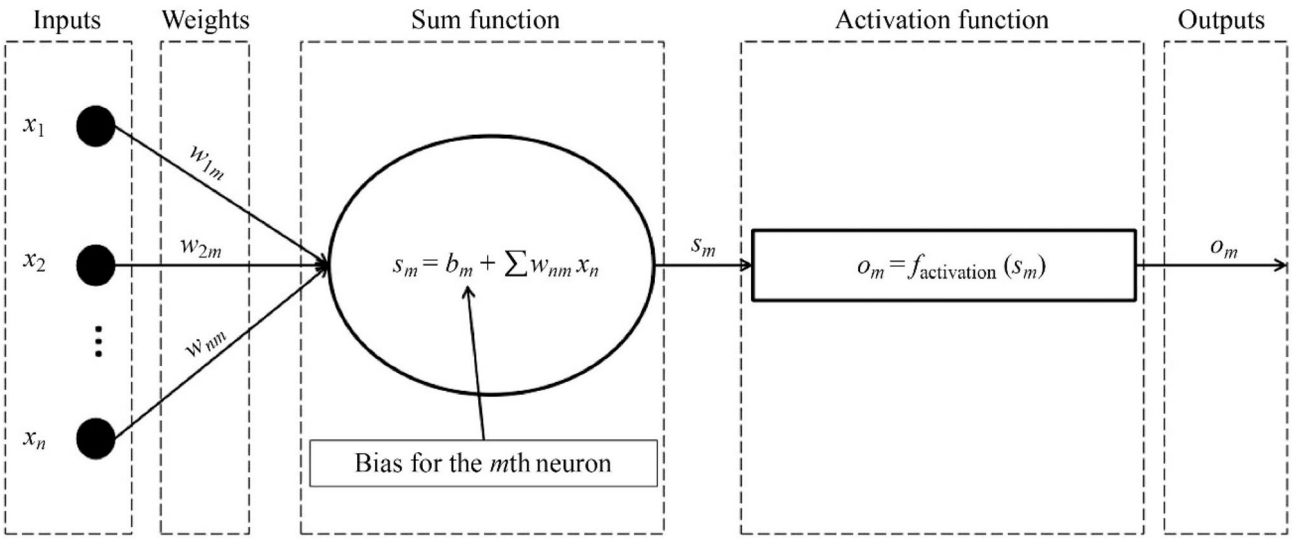

Fig. 3 Data processing of the mth neuron in hidden or output layer

less than 81 groups and the data were complete and correct. Hence, the Levenberg-Marquardt backpropagation algorithm is the most appropriate choice of training algorithm in this study. Other training algorithms were also tested for the purpose of comparison.

(v) Learning rate. For many training algorithms, the learning rate is adaptive. The learning rate was generally set in the range 0.1–0.9 for the training algorithms that required an explicit learning rate.

(vi) Tolerable error. The tolerable error, which represents the goal mean square error (MSE) between the outputs from the model output layer and the corresponding target outputs, was often set as 10^{-6} or 0.

(vii) Minimum MSE gradient. When the difference between the current MSE for all input vectors and the old MSE before a training epoch is less than the minimum MSE gradient, the training process ends.

(viii) Maximum iterations. The aim of maximum iterations was to avoid the occurrence of an infinite weight updating loop if the model cannot converge. If the convergence rate of the training algorithm is empirically high, the maximum iteration is often set as a smaller value and vice versa. Example smaller and larger values are 1 000 and 10 000, respectively.

Step 2 Assign the initial weight values for all connections and bias values for all neurons in hidden and output layers randomly.

Step 3 Input an input vector to the neural network model. The input vector in this paper was $[\varphi_{\text{SiC}}, V_{\text{c}}, F_{\text{r}}, D_{\text{c}}]$.

Step 4 Based on the input vector in Step 3, the output values for all neurons in the hidden layer and output layer are calculated via Eq. (1). In particular, the output of any neuron in the input layer is equal to the input to this neuron.

$$o_m^k = f_{\text{activation}}\left(\left(\sum_{n=1}^{N} w_{nm}\, o_n^{k-1}\right) + b_m^k\right), \tag{1}$$

where o_m^k is the output of the mth neuron in the layer under consideration; o_n^{k-1} is the output of the nth neuron in the preceding layer and N is the number of neurons in the preceding layer; w_{mn} is the weight value of the connection between the mth neuron in the layer under consideration and the nth neuron in the preceding layer; b_m^k is the bias value for the mth neuron in the layer under consideration; $f_{\text{activation}}$ is the activation function. In this paper, the SoftMax function and pure linear function were set as the activation functions for the hidden layer(s) and output layer, respectively. The explanation of the SoftMax function and pure linear function is as follows. SoftMax function: $f(x) = \frac{e^x}{\sum_{m=1}^{M} e^{x_m}}$ (M and m are the number of neurons and the mth neuron in the layer under consideration, respectively); pure linear function: $f(x) = x$.

Step 5 Obtain the output value of one neuron in the output layer and calculate the error and square error between this output value ($R_{\text{a\_predicted}}$) and the corresponding target output value ($R_{\text{a\_target}}$) via Eqs. (2) and (3), respectively.

$$E_i = R_{a\_predicted\_i} - R_{a\_target\_i}, \quad (2)$$

$$S_i = (R_{a\_predicted\_i} - R_{a\_target\_i})^2, \quad (3)$$

where E_i and S_i are the error and squared error between $R_{a\_predicted\_i}$ and $R_{a\_target\_i}$ for the ith input vector, respectively; $R_{a\_predicted\_i}$ and $R_{a\_target\_i}$ are the calculated output value and target output value of one neuron in the output layer for the ith input vector, respectively.

Step 6 Adjust weights and biases based on the various errors in Step 5 and the training algorithm. Levenberg-Marquardt backpropagation was selected as the training algorithm, which provided the rule (as shown in Eqs. (4)–(5)) below, for adjusting

$$\boldsymbol{W}_{bnew} = \boldsymbol{W}_{bold} + \left[\boldsymbol{J}^T + \mu \boldsymbol{I}\right]^{-1} \boldsymbol{J}^T E_i, \quad (4)$$

$$\boldsymbol{J} = \left[\frac{\partial E_i}{\partial \boldsymbol{W}_{b\_1}}, \cdots, \frac{\partial E_i}{\partial \boldsymbol{W}_{b\_P}}\right], \quad (5)$$

where $\boldsymbol{W}_{bnew}$ is the new weights-bias matrix which consists of all weights and biases updated over $\boldsymbol{W}_{bold}$ after the ith input vector is used for training; $\boldsymbol{J}$ is the Jacobian matrix; P is the number of elements in the $\boldsymbol{W}_b$ matrix; $\boldsymbol{I}$ is a unit matrix; and μ is an adaptive factor influenced by the S_i.

Step 7 Execute Steps 3 to 6 for an intact epoch and observe whether the current E_{ms} (mean squared error) for all input vectors, calculated using Eq.(6), is less than the tolerable error or whether the difference between the current E_{ms} and the E_{ms} before this training epoch is less than the minimum MSE gradient; if so, proceed to Step 8 and if not, repeat Steps 3 to 7 until the maximum iteration count is reached.

$$E_{ms} = \frac{\sum_{i=1}^{N_{train}} \left(R_{a\_predicted\_i} - R_{a\_target\_i}\right)^2}{N_{train}}, \quad (6)$$

where N_{train} is the number of input vectors in training dataset (or the size of the training dataset).

Step 8 Stop iteration and fix all model parameters, including weights and bias values.

Step 9 Validate the model using the validation dataset and calculate the E_{msv} via Eq. (7). If E_{msv} is not more than the tolerable error, then the neural network has been successfully built. Otherwise, the model is considered as overfitting; the model parameters should be changed and all the above steps repeated.

$$E_{msv} = \frac{\sum_{i=1}^{N_{val}} \left(R_{a\_predicted\_i} - R_{a\_target\_i}\right)^2}{N_{val}}, \quad (7)$$

where E_{msv} is the mean squared error between the outputs and target outputs for all input vectors in the validation dataset; and N_{val} is the size of the validation dataset.

In this experiment, 8 out of 81 groups of data (see Table 2) were randomly selected as the validation dataset and the rest were used for training. After sufficient attempts with different model parameters, an ANN surface roughness prediction model, named Model 1 in Table 3, with better performance was successfully built and selected. Models 2 and 3 were representative of this model but with inferior performance. Using the successfully developed prediction model, the user could obtain surface roughness during the process of milling rather than after the milling process, based on the cutting parameters. Obtaining the roughness at this earlier stage may have limited significance in practical production. However, if the predicted roughness provides the user with some information on how to adjust cutting parameters to achieve a desired roughness, the significance of the roughness prediction model would greatly improve. Therefore, a roughness control model was also developed, based on the roughness prediction model.

3.2 Development of the roughness control model

Based on the selected roughness prediction model described in the above section, a roughness control model that could determine cutting parameters corresponding to a specific desired roughness value was developed. Using this control model, the roughness of the milled surface could be specified via control of the cutting parameters. The flow diagrams in Fig. 4 describe the roughness control model algorithms, which can achieve different functions with different inputs. The objective of the algorithms in Figs. 4a–c is to determine the cutting parameters for a specific roughness, minimum roughness, and roughness under a certain value, respectively, within a given cutting parameters' range. The control model can be applied to improve the production efficiency when the requirements for the milled surface are special. For example, when a manufacturer requires a part with a specific friction factor, i.e., a particular roughness value, the control model with Algorithm (a) in Fig. 4 can assist in milling this manufacture part. The industry field typically requires a roughness below a certain value or the smallest roughness value possible. The control model with algorithms (b) and (c) in Fig. 4 contributes to satisfying such requirements.

4 Results and discussions

4.1 Evaluation of roughness prediction model results

To maintain the objectivity of the evaluation, further experiments were conducted after two months to obtain test data for evaluating the performance of the selected ANN surface roughness prediction model (Model 1 in Table 3). The test data and predicted surface roughness values can be

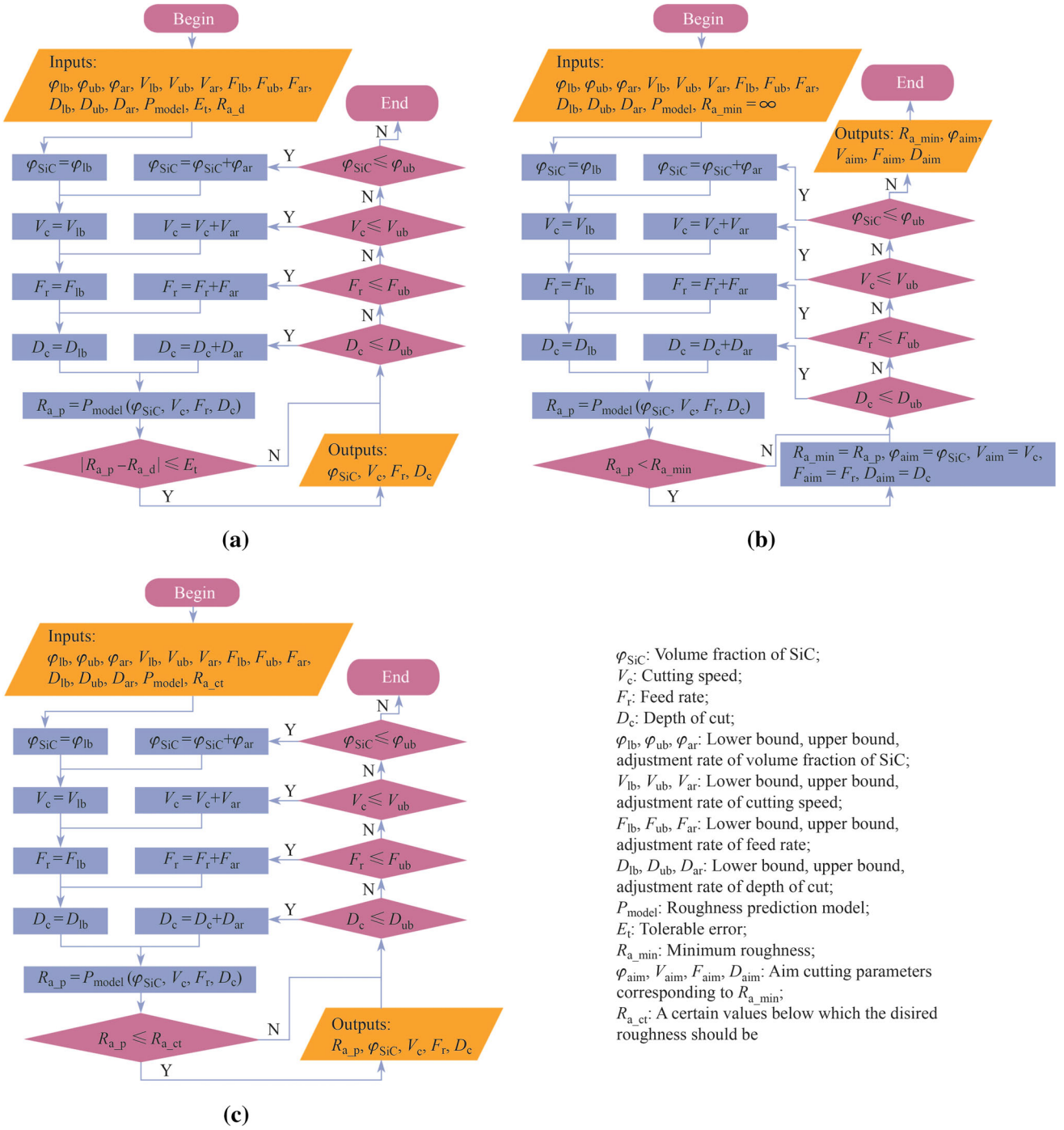

Fig. 4 Algorithms of surface roughness control model

seen in Table 4. Figure 5 shows the difference between target and predicted values of surface roughness and visually illustrates the insignificance of the difference. Here, mean relative error (MRE) was selected as the metric for measuring the difference. The expression and mathematical implications of MRE are easy to understand and MRE is often used by researchers to evaluate the roughness prediction model [19]. By calculating the mean relative error based on Eq. (8) (2.08%), it can be concluded that this ANN surface roughness prediction model is reliable and feasible.

$$E_{mr}=\frac{1}{N_{test}}\sum_{i=1}^{N_{test}}\left|\frac{R_{a\_predicted\_i}-R_{a\_measured\_i}}{R_{a\_measured\_i}}\right|, \tag{8}$$

Table 4 Test data and evaluation results for roughness prediction model

No.	φ_{SiC}/%	$V_c/(m \cdot min^{-1})$	$F_r/(mm \cdot r^{-1})$	D_c/mm	Measured R_a/μm	Predicted R_a/μm	Error/μm
1	0	55	0.15	0.07	0.174	0.177	0.003
2	0	70	0.25	0.10	0.230	0.237	0.007
3	0	85	0.35	0.13	0.342	0.340	0.002
4	15	55	0.25	0.13	0.349	0.359	0.010
5	15	70	0.35	0.07	0.452	0.449	0.003
6	15	85	0.15	0.10	0.181	0.188	0.007
7	25	55	0.35	0.10	0.629	0.613	0.016
8	25	70	0.15	0.13	0.234	0.234	0.000
9	25	85	0.25	0.07	0.265	0.274	0.009

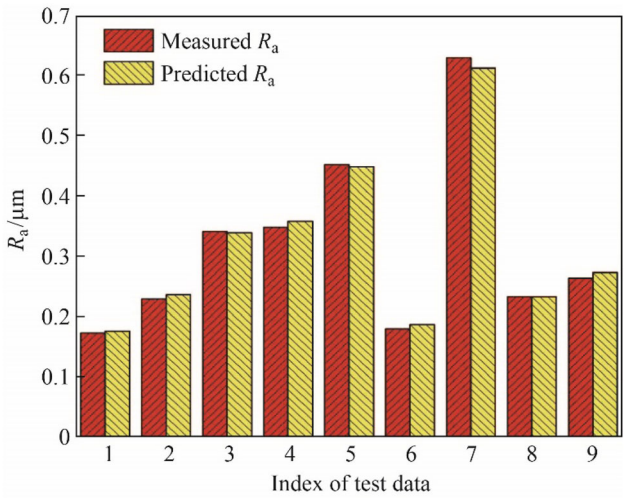

Fig. 5 Evaluation results of surface prediction model

where E_{mr} is the mean relative error; $R_{a\_predicted\_i}$ and $R_{a\_measured\_i}$ are the predicted and measured R_a of the ith test data, respectively; and N_{test} is the size of the test data.

4.2 Evaluation results of roughness control model

Further experiments were conducted to evaluate the efficiency and accuracy of this roughness control model. Initially, the ranges and adjustment rate of the cutting and other system parameters were set based on Table 5. We subsequently determined the cutting parameters corresponding to a specific or minimum roughness via this roughness control model and recorded the time cost. Finally, these parameters were input into the CNC machine and the average roughness of the machined workpiece was measured. The test data are listed in Table 6. Figure 6 shows the comparison of desired and measured roughness. Based on Table 6 and Fig. 6, the average time cost by the control system can be obtained (36.33 s). The mean squared error and mean relative error between desired roughness and measured roughness is 1.02×10^{-4} and 2.91%, respectively; this proves that the roughness control model has satisfactory efficiency and accuracy. It is of further note that the value of E_t in Table 5 should have been set to 0.001 μm as the resolution of the roughness tester is 0.001 μm. However, too many groups of the corresponding cutting parameters were output by the control model when E_t was equal to 0.001 μm, dramatically

Table 5 Parameter settings for the roughness control model

Parameter	Value		
	Lower bound	Upper bound	Adjustment rate
Cutting parameter			
φ_{SiC}/%	0	25	5
$V_c/(m \cdot min^{-1})$	40	100	5
$F_r/(mm \cdot r^{-1})$	0.10	0.40	0.05
D_c/mm	0.05	0.15	0.01
System parameter			
P_{model}	The successfully built roughness prediction Model 1 in Table 3		
E_t	0.000 1 μm		

Table 6 Test data and evaluation results for roughness control model

No.	Desired R_a/μm	Obtained cutting parameters				Time of cost/s	Measured R_a/μm	Error/μm
		φ_{SiC}/%	$V_c/(m \cdot min^{-1})$	$F_r/(mm \cdot r^{-1})$	D_c/mm			
1	0.2	0	85	0.25	0.06	32.97	0.215	0.015 0
		15	50	0.15	0.06		0.201	0.001 0
		15	60	0.15	0.08		0.192	0.008 0
2	0.3	0	100	0.35	0.11	39.69	0.304	0.004 0
		25	75	0.25	0.07		0.310	0.010 0
		25	90	0.25	0.13		0.306	0.006 0
3	0.4	25	70	0.30	0.07	37.83	0.406	0.006 0
		25	100	0.40	0.06		0.393	0.007 0
4	0.5	15	85	0.40	0.10	33.65	0.478	0.022 0
	0.7	–	–	–	–	32.94	–	–
5	Minimum roughness (0.127 5)	0	100	0.10	0.05	40.89	0.131	0.003 5

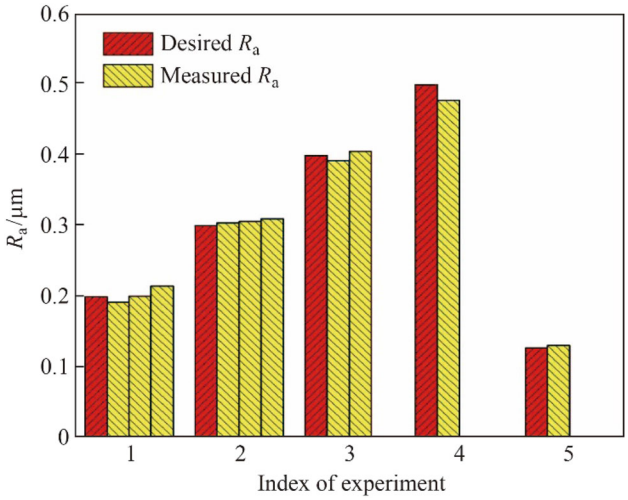

Fig. 6 Evaluation results of roughness control system

increasing the workload of the milling process. Therefore, E_t was set to 0.000 1 μm in this experiment. Moreover, other parameters' values, apart from P_{model}, can be set to different values dependent on the users' requirements. For example, decreasing the range or enlarging the adjustment rate of cutting parameters can improve the efficiency of the control model.

4.3 Results of assessing cutting parameters' effects on surface roughness

4.3.1 Assessing results based on the ANN model

Various researchers [11–13, 43] have used experimental data to directly investigate the influence of cutting parameters on surface roughness via the ANOVA or regression tree method. Even though the ANOVA and regression tree method, based on mathematical analysis, could provide more detailed information compared to the 2D- or 3D-charts, the size of the data from the experiment was limited in general. The accuracy of the analysis result would be influenced based on such limited data. A reliable ANN surface roughness prediction model could describe the accurate mathematical relationship between the cutting parameters and surface roughness. However, the ANN model was a "black box" that was difficult to provide with

Table 7 Example data for analyzing a single parameter's influence on roughness

No.	φ_{SiC}/%	$V_c/(m \cdot min^{-1})$	$F_r/(mm \cdot r^{-1})$	D_c/mm	Predicted R_a/μm
1	15	40	0.25	0.1	0.348 0
2	15	41	0.25	0.1	0.347 7
3	15	42	0.25	0.1	0.347 3
⋮	⋮	⋮	⋮	⋮	⋮
59	15	99	0.25	0.1	0.242 2
61	15	100	0.25	0.1	0.240 5

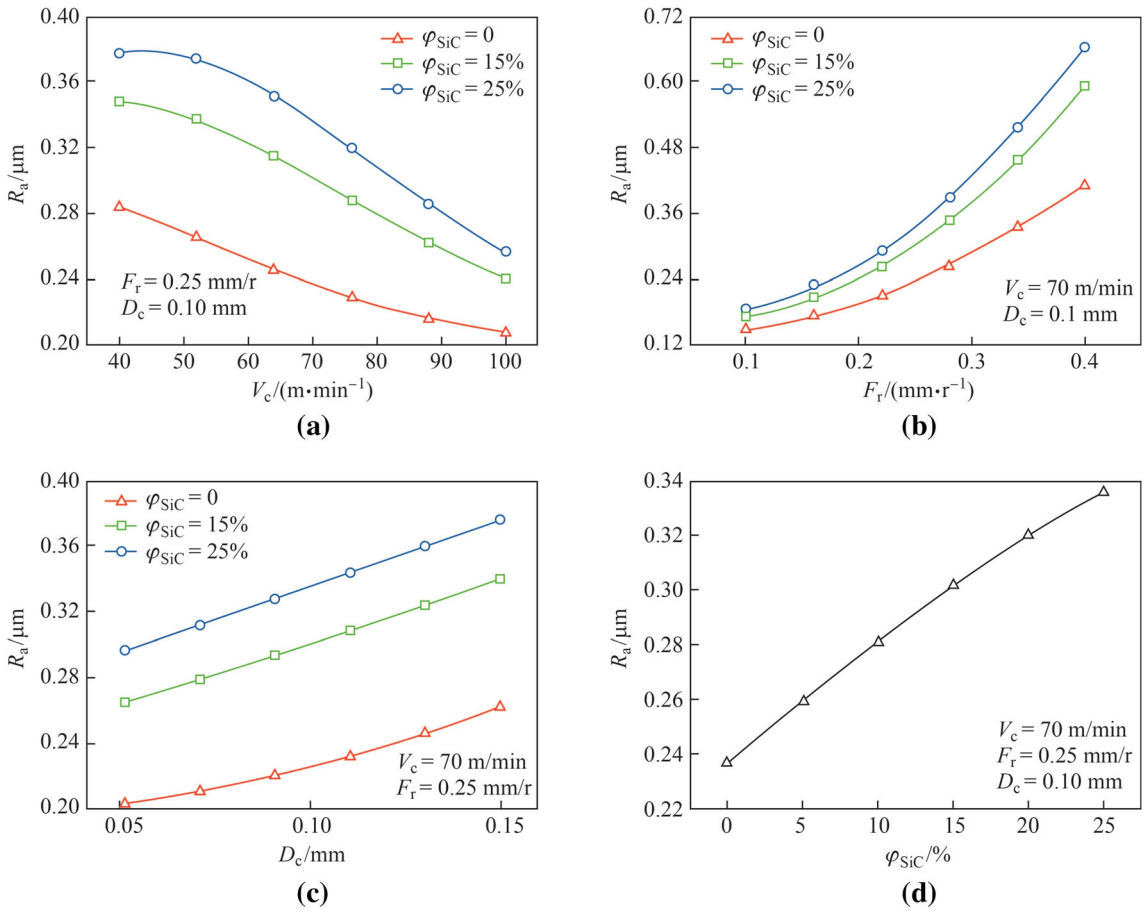

Fig. 7 Influences of **a** cutting speed, **b** feed rate, **c** depth of cut, and **d** volume fraction of SiC on average roughness

Table 8 Example data for analyzing multiple parameters' influence on roughness

No.	φ_{SiC}/%	V_c/(m · min^{-1})	F_r/(mm · r^{-1})	D_c/mm	Predicted R_a/μm
1	15	40	0.10	0.1	0.187 5
2	15	40	0.11	0.1	0.193 0
3	15	40	0.12	0.1	0.199 1
⋮	⋮	⋮	⋮	⋮	⋮
31	15	40	0.40	0.1	0.707 1
32	15	41	0.10	0.1	0.187 1
33	15	41	0.11	0.1	0.192 7
⋮	⋮	⋮	⋮	⋮	⋮
1891	15	100	0.40	0.1	0.411 9

the visualized influences of cutting parameters on roughness. In this paper, the ANN model was used to generate sufficient data for analyzing the cutting parameters' influence on average roughness via 2D- and 3D-charts. For example, if the influence of cutting speed on surface roughness was expected to be studied, data could be generated, as in Table 7. An analysis curve, such as in Fig. 7a, could then be obtained. If the influence of the interaction of cutting speed and feed rate on roughness was intended for investigation, the data could be generated, as in Table 8. An analysis curve, such as in Fig. 8a, could then be obtained accordingly.

Similarly, the curves showing the influence of feed rate, depth of cut, volume fraction of SiC, or the interaction of

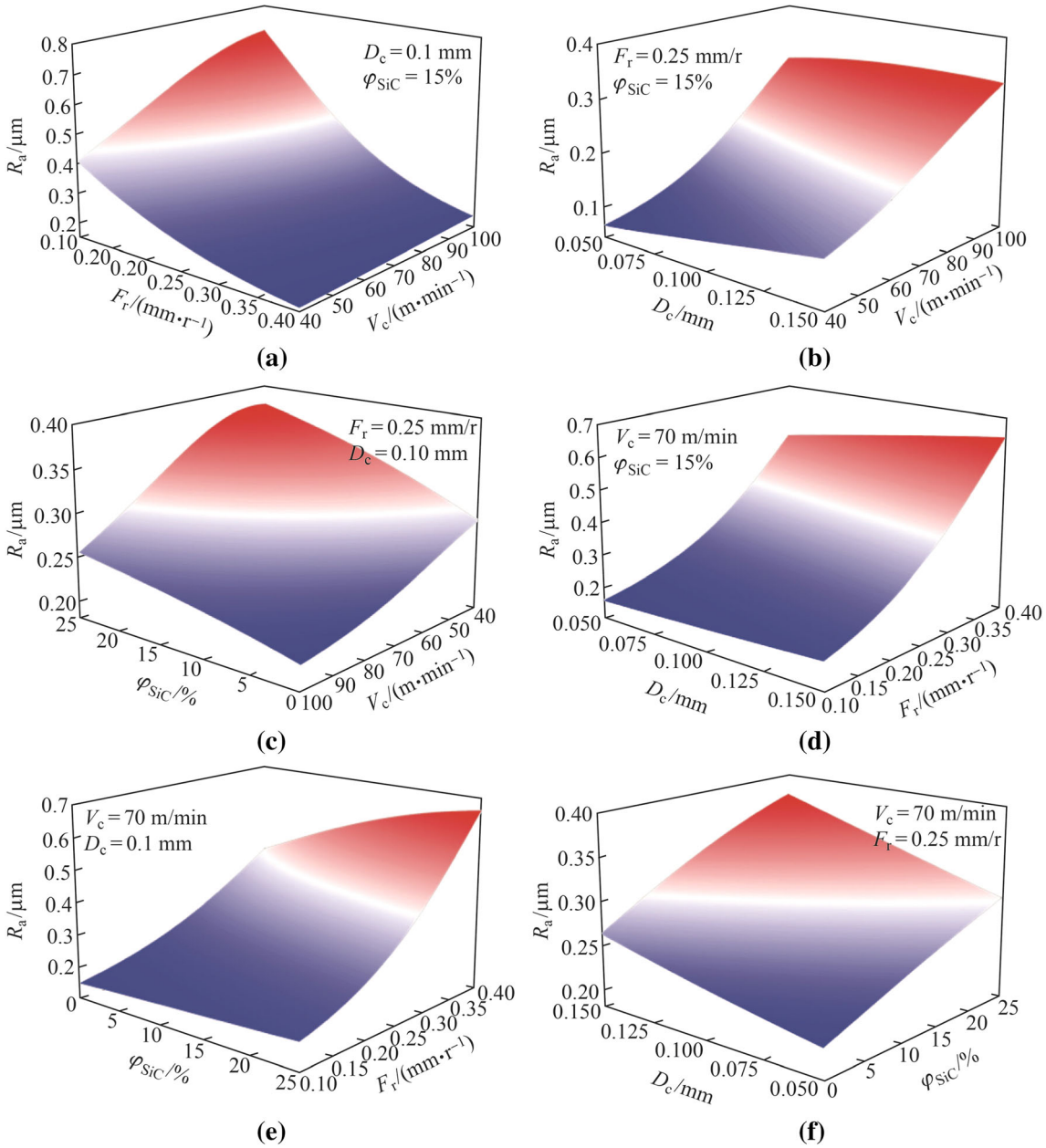

Fig. 8 Influences of interaction of two cutting parameters on average roughness

two different cutting parameters, on surface roughness were also generated, shown in Figs. 7 and 8.

From Fig. 7a, it can be seen that the average surface roughness value decreases with increasing cutting speed when the feed rate and depth of cut are 0.25 mm/r and 0.1 mm, respectively, regardless of the volume fraction of SiC. The decreasing speed of roughness value with increasing cutting speed increases with the increase of volume fraction of SiC when the cutting speed exceeds a certain value. Figure 7b shows that the roughness value increases with increasing feed rate when the cutting speed and depth of cut are 70 mm/min and 0.1 mm, respectively. The roughness value has an approximately exponential relationship to the feed rate when the feed rate is within the proper range. According to Fig. 7c, the roughness value increases with the depth of cut when the cutting speed and feed rate are 70 mm/min and 0.25 mm/r, respectively. There is a linear relationship between the roughness value and depth of cut and the slope of the line is approximately 0.515 μm/mm, 0.754 μm/mm, and 0.797 μm/mm when the volume fraction of SiC is 0, 15%, and 25%, respectively. Similarly, it can be seen from Fig. 7d that the roughness value also increases linearly with the increase of volume of fraction of SiC, and the line slope is approximately

Table 9 Measure of the significance of the parameter's influence on roughness

Two parameters	The measure to decide which one is the more significant influence on roughness
V_c and F_r	Variation of roughness for 0.15 mm/r feed rate variation = significance of feed rate
	Variation of roughness for 30 m/min cutting speed variation = significance of cutting speed
V_c and φ_{SiC}	Variation of roughness for 30 m/min cutting speed variation = significance of cutting speed
	Variation of roughness for 10% (volume fraction) of SiC variation = significance of depth of cut
φ_{SiC} and D_c	Variation of roughness for 10% (volume fraction) of SiC variation = significance of depth of cut
	Variation of roughness for 0.05 mm depth of cut variation = significance of depth of cut

0.004 μm/% when the cutting speed, feed rate, and depth of cut are 70 mm/min, 0.25 mm/r, and 0.1 mm, respectively.

Figure 8 describes the effect of the interaction between two different cutting parameters on the average surface roughness value. The relation between roughness value and the interaction of cutting speed and feed rate is shown in Fig. 8a. From this figure, it can be seen that the influence of feed rate on roughness value is more significant than that of cutting speed and the influence of cutting speed becomes more significant as the feed rate increases. Figure 8c shows that the significance of the influence of cutting speed on roughness value is greater than that of the volume of SiC. Figure 8f suggests that the importance of the influence of volume of SiC on roughness value is slightly higher than that of the depth of cut. Table 9 presents the measure of judging which parameter's influence on roughness value is the most significant. To summarize, the feed rate has the most significant influence on roughness value, followed by cutting speed and volume of SiC. The depth of cut has the smallest influence on roughness value. Moreover, it can be seen from Fig. 8b that the influence of the depth of cut on the roughness value is always stable and small, regardless of the value of cutting speed. From Fig. 8d, we can see that the increasing speed of roughness value with the increasing depth of cut increases slightly with the increase in feed rate. Figure 8e illustrates that the increasing speed of roughness value with the increase in volume fraction of SiC increases with the increase in feed rate.

4.3.2 Assessing results based on ANOVA

ANOVA has often been used to determine which of the cutting parameters' influence on roughness is the most significant [12, 13, 44]. ANOVA is a method of portioning variability in an experiment into identifiable sources of variation and the associated degrees of freedom. In statistics, an *F* test is used for analyzing the significant effect of the parameters on the quality characteristic. Table 10 gives

Table 10 ANOVA table

Source of validation	Degrees of freedom	Sum of squares	Mean square	*F*-value	Contribution/%	*P*-value
φ_{SiC}	2	0.085 15	0.042 58	201.40	3.11	0.000
V_c	2	0.266 34	0.133 17	629.91	9.74	0.000
F_r	2	2.046 06	1.023 03	4 839.16	74.80	0.000
D_c	2	0.072 44	0.036 22	171.32	2.65	0.000
$\varphi_{SiC}V_c$	4	0.010 23	0.002 56	12.10	0.37	0.000
$\varphi_{SiC}F_r$	4	0.041 39	0.010 35	48.94	1.51	0.000
$\varphi_{SiC}D_c$	4	0.001 28	0.000 32	1.52	0.05	0.244
V_cF_r	4	0.163 73	0.040 93	193.62	5.99	0.000
V_cD_c	4	0.001 46	0.000 36	1.72	0.05	0.194
F_rD_c	4	0.021 63	0.005 41	25.57	0.79	0.000
$\varphi_{SiC}V_cF_r$	8	0.012 23	0.001 53	7.23	0.45	0.000
$\varphi_{SiC}V_cD_c$	8	0.001 23	0.000 15	0.73	0.04	0.667
$\varphi_{SiC}F_rD_c$	8	0.004 51	0.000 56	2.67	0.16	0.045
$V_cF_rD_c$	8	0.004 22	0.000 53	2.49	0.15	0.057
Error	16	0.003 38	0.000 21		0.12	
Total	80	2.735 27			100.00	

Table 11 Data for ANOVA

No.	φ_{SiC}/%	V_c/(m·min^{-1})	F_r/(mm·r^{-1})	D_c/mm	Predicted R_a/μm	No.	φ_{SiC}/%	V_c/(m·min^{-1})	F_r/(mm·r^{-1})	D_c/mm	Predicted R_a/μm	No.	φ_{SiC}/%	V_c/(m·min^{-1})	F_r/(mm·r^{-1})	D_c/mm	Predicted R_a/μm
1	5	40	0.10	0.05	0.170	28	15	40	0.10	0.05	0.187	55	25	40	0.10	0.05	0.178
2	5	40	0.10	0.10	0.180	29	15	40	0.10	0.10	0.196	56	25	40	0.10	0.10	0.185
3	5	40	0.10	0.15	0.192	30	15	40	0.10	0.15	0.192	57	25	40	0.10	0.15	0.212
4	5	70	0.10	0.05	0.148	31	15	70	0.10	0.05	0.177	58	25	70	0.10	0.05	0.171
5	5	70	0.10	0.10	0.157	32	15	70	0.10	0.10	0.181	59	25	70	0.10	0.10	0.172
6	5	70	0.10	0.15	0.169	33	15	70	0.10	0.15	0.197	60	25	70	0.10	0.15	0.200
7	5	100	0.10	0.05	0.134	34	15	100	0.10	0.05	0.164	61	25	100	0.10	0.05	0.164
8	5	100	0.10	0.10	0.145	35	15	100	0.10	0.10	0.175	62	25	100	0.10	0.10	0.168
9	5	100	0.10	0.15	0.160	36	15	100	0.10	0.15	0.180	63	25	100	0.10	0.15	0.180
10	5	40	0.25	0.05	0.273	37	15	40	0.25	0.05	0.295	64	25	40	0.25	0.05	0.353
11	5	40	0.25	0.10	0.308	38	15	40	0.25	0.10	0.349	65	25	40	0.25	0.10	0.382
12	5	40	0.25	0.15	0.348	39	15	40	0.25	0.15	0.389	66	25	40	0.25	0.15	0.419
13	5	70	0.25	0.05	0.231	40	15	70	0.25	0.05	0.242	67	25	70	0.25	0.05	0.294
14	5	70	0.25	0.10	0.260	41	15	70	0.25	0.10	0.304	68	25	70	0.25	0.10	0.341
15	5	70	0.25	0.15	0.293	42	15	70	0.25	0.15	0.355	69	25	70	0.25	0.15	0.406
16	5	100	0.25	0.05	0.193	43	15	100	0.25	0.05	0.193	70	25	100	0.25	0.05	0.227
17	5	100	0.25	0.10	0.220	44	15	100	0.25	0.10	0.234	71	25	100	0.25	0.10	0.259
18	5	100	0.25	0.15	0.254	45	15	100	0.25	0.15	0.265	72	25	100	0.25	0.15	0.299
19	5	40	0.40	0.05	0.498	46	15	40	0.40	0.05	0.604	73	25	40	0.40	0.05	0.718
20	5	40	0.40	0.10	0.576	47	15	40	0.40	0.10	0.714	74	25	40	0.40	0.10	0.778
21	5	40	0.40	0.15	0.651	48	15	40	0.40	0.15	0.785	75	25	40	0.40	0.15	0.860
22	5	70	0.40	0.05	0.418	49	15	70	0.40	0.05	0.568	76	25	70	0.40	0.05	0.636
23	5	70	0.40	0.10	0.478	50	15	70	0.40	0.10	0.577	77	25	70	0.40	0.10	0.658
24	5	70	0.40	0.15	0.536	51	15	70	0.40	0.15	0.664	78	25	70	0.40	0.15	0.681
25	5	100	0.40	0.05	0.321	52	15	100	0.40	0.05	0.346	79	25	100	0.40	0.05	0.404
26	5	100	0.40	0.10	0.371	53	15	100	0.40	0.10	0.354	80	25	100	0.40	0.10	0.427
27	5	100	0.40	0.15	0.420	54	15	100	0.40	0.15	0.515	81	25	100	0.40	0.15	0.457

the ANOVA results for average surface roughness based on the data in Table 11.

From Table 10, it can be concluded that feed rate is the dominant parameter influencing the average surface roughness, with a percentage contribution of 74.80%, followed by cutting speed, volume fraction of SiC, and depth of cut with percentage contributions of 9.74%, 3.11%, and 2.65% respectively. This result by the ANOVA is consistent with the visual analysis results based on the ANN roughness prediction model. Regarding the interaction of parameters, the interaction of cutting speed and feed rate has the most significant effects on roughness, with a percentage contribution of 5.99%, followed by the interaction of volume fraction of SiC and feed rate, with a 1.51% contribution.

4.4 Discussion

This section explains why a higher cutting speed, lower feed rate, smaller volume fraction of SiC, and lower depth of cut can lead to a lower roughness value during milling Al/SiC composites. According to Section 2.3, the main component of the Al/SiC composite materials used in this experiment is aluminum, implying that these materials are more similar to plastic materials. When milling plastic materials, the formation of built-up edge (BUE) is an important phenomenon that influences the roughness of the milled surface. At low cutting speeds, BUE and chip fracture form readily, resulting in a rough surface. With an increase in cutting speed, the BUE begins to vanish, chip fracture decreases, and hence the roughness decreases. Furthermore, the increasing depth of cut leads to a higher normal pressure and seizure on the rake face, which promotes formation of the BUE. When the feed rate increases, the BUE forms so quickly that the removal speed of chip fracture is much lower than its formation speed. Therefore, the roughness increases with increasing depth of cut or feed rate. During the process of milling Al/SiC composites, soft Al matrix and hard SiC particles are cut alternately, causing tool vibration. Hence, the formation of the milled surface is not only influenced by the common cutting parameters, such as cutting speed, feed rate, and depth of cut but is also greatly influenced by the hard SiC particles. The rotation, pressed-in, pulled out, and fracture of SiC particles after milling contributes to the formation of micro-cracks, pits, swellings, and cavities [7]. The increase of the volume fraction of SiC increases the formation probability of these defects and hence the roughness increases.

5 Conclusions

In conclusion, an accurate roughness prediction and control model was well developed based on the ANN method for milling Al/SiC composites. This suggests that machine learning methods are reliable and effective for solving problems in the field of machining. Introducing more machine learning methods to the industry field should be encouraged. High-precision milling of the Al/SiC composite is a difficult task. However, we can control the roughness to a specific value or range using the roughness control model, which contributes to widening the potential application of such materials. Furthermore, an in-depth analysis of the cutting parameters' influences on roughness was conducted in this study. The following presents the various exciting and novel findings of this study.

(i) The Levenberg-Marquardt backpropagation training algorithm is reliable and efficient for developing the roughness prediction model for machining.
(ii) Among the factors investigated in this paper, the feed rate has the most significant influence on surface roughness, followed by cutting speed and volume fraction of SiC.
(iii) The speed of roughness decreases with cutting speed and increases with an increase in volume fraction of SiC and feed rate.
(iv) Surface roughness has an approximately exponential relation to the feed rate when the feed rate is within a certain range.
(v) The relation between surface roughness and depth of cut is approximately linear, as is the relation between roughness and volume fraction of SiC.

Acknowledgements This work was supported by the National High Technology Research and Development Plan of China (Grant No. 2015AA043505), the Equipment Advanced Research Funds (Grant No. 61402100401), the Equipment Advanced Research Key Laboratory Funds (Grant No. 6142804180106) and Shenzhen Fundamental Research Funds (Grant No. JCYJ20180508151910775).

Appendix

See Tables 12, 13, 14, 15, 16, 17, 18, 19, 20, 21, 22, and 23.

Table 12 Trained weights of connections between neurons in the input and hidden layer of Model 1

*m*th neuron in the hidden layer	w_{mn}			
	*n*th neuron in the input layer			
	1	2	3	4
1	1.017 589 213 060 440 0	0.863 445 286 458 416	− 0.330 939 553 640 245	− 0.059 180 991 210 196 0
2	0.087 754 617 396 610 7	− 0.544 277 024 420 964	− 0.265 088 274 193 894	− 0.296 575 362 795 697 0
3	− 0.027 544 590 829 428 8	0.943 183 213 345 640	0.386 853 517 682 408	0.069 105 989 222 525 3
4	− 0.563 462 234 809 686 0	0.501 484 695 543 195	− 0.534 129 349 227 771	− 0.169 088 343 746 247 0
5	0.750 727 921 402 287 0	− 0.523 671 687 926 136	1.004 873 469 718 330	− 0.097 307 665 808 396 4
6	0.742 115 967 957 793 0	− 1.518 660 500 798 010	− 0.912 847 028 631 556	− 0.466 465 775 340 742 0
7	0.470 689 352 311 570 0	1.532 687 479 703 330	− 0.459 260 066 479 935	− 0.441 407 562 353 176 0
8	0.249 714 338 890 135 0	0.044 143 877 764 294	− 1.228 634 016 998 820	− 0.453 162 627 256 598 0
9	− 0.945 979 972 345 994 0	− 0.254 776 933 181 228	0.468 244 460 182 997	− 0.593 225 046 641 105 0

Table 13 Weights of connections between neurons in the hidden and output layer of Model 1

$n_{\mathbf{th}}$ neuron in the hidden layer	w_{mn} (*m*th neuron in the output layer, $m = 1$)
1	− 0.203 481 663 022 754
2	0.893 604 432 333 132
3	0.909 538 682 572 744
4	− 0.948 614 299 262 459
5	2.311 361 137 406 700
6	− 0.533 626 377 004 459
7	− 0.707 609 156 773 631
8	− 0.650 662 401 597 233
9	− 0.462 132 046 445 955

Table 14 Biases of neurons in the hidden layer of Model 1

*m*th neuron in the hidden layer	b_m
1	0.567 921 472 505 165
2	− 0.070 663 769 287 509
3	− 0.200 999 139 853 644
4	0.337 329 717 218 552
5	0.281 363 388 420 558
6	− 0.027 017 995 211 923
7	0.102 025 920 162 819
8	1.683 367 752 712 950
9	− 0.453 464 876 665 677

Table 15 Biases of neurons in the output layer of Model 1

	*m*th neuron in the output layer ($m = 1$)
b_m	0.567 921 472 505 165

Table 16 Trained weights and biases of connections between neurons in the input and hidden layer of Model 2

*m*th neuron in the hidden layer	w_{mn}			
	*n*th neuron in the input layer			
	1	2	3	4
1	0.333 062 533 482 354 00	− 0.669 929 278 358 898	− 0.082 981 876 711 817 2	0.186 638 062 025 992
2	0.406 927 229 515 461 00	− 0.407 159 204 165 448	1.178 805 199 628 140 0	0.319 046 218 050 420
3	0.131 433 605 769 185 00	0.425 163 770 931 838	0.546 936 973 434 565 0	0.747 451 106 781 039
4	− 0.712 312 846 373 877 00	− 0.362 670 660 588 039	0.611 434 399 420 019 0	0.441 350 512 610 603
5	0.042 118 540 173 047 20	0.905 484 006 607 461	− 0.749 583 820 409 598 0	− 0.381 709 490 224 342
6	0.222 720 165 880 150 00	0.405 493 198 562 445	− 0.696 422 527 572 816 0	0.017 369 337 958 777
7	− 1.044 946 520 360 790 00	− 0.605 247 580 547 393	− 0.751 776 084 836 262 0	− 0.477 307 125 596 477
8	0.003 535 162 671 403 27	0.102 405 437 268 855	− 0.770 228 065 696 404 0	0.384 781 851 585 763
9	0.684 357 463 538 259 00	0.799 245 174 944 205	− 1.169 035 941 829 800 0	− 0.712 623 450 617 290

Table 17 Weights of connections between neurons in the hidden and output layer of Model 2

*n*th neuron in the hidden layer	w_{mn} (*m*th neuron in the output layer, $m = 1$)
1	− 0.367 917 589 384 117 00
2	1.378 204 354 180 820 00
3	− 0.436 266 961 244 193 00
4	− 0.391 868 678 305 883 00
5	− 0.399 323 095 161 256 00
6	− 0.656 778 272 594 529 00
7	− 0.774 456 822 418 629 00
8	0.004 746 512 709 425 99
9	− 0.881 874 781 298 528 00

Table 18 Biases of neurons in the hidden layer of Model 2

*m*th neuron in the output layer	b_m
1	0.371 130 002 742 130
2	0.932 020 345 350 965
3	0.332 015 072 928 862
4	− 0.362 807 748 256 077
5	0.164 239 345 525 504
6	− 0.030 060 084 132 496
7	− 0.753 800 000 855 562
8	0.467 431 236 169 857
9	0.466 655 670 783 005

Table 19 Biases of neurons in the output layer of Model 2

	*m*th neuron in the output layer ($m = 1$)
b_m	− 0.379 230 855 865 313

Table 20 Trained weights and biases of connections between neurons in the input and hidden layer of Model 3

*m*th neuron in the hidden layer	w_{mn}			
	*n*th neuron in the input layer			
	1	2	3	4
1	− 0.115 626 564 551 590	− 0.671 382 273 326 524	− 0.356 022 428 125 678 0	0.031 598 683 565 010 7
2	− 1.954 920 587 347 450	1.052 402 461 488 520	0.882 338 185 371 201 0	0.069 877 475 651 290 5
3	0.650 895 393 747 986	− 0.730 401 091 279 281	− 1.423 364 009 971 040 0	− 0.223 564 770 489 663 0
4	− 0.517 719 243 605 188	1.144 950 461 730 040	− 1.019 919 175 977 180 0	− 0.176 161 436 359 717 0
5	0.395 041 199 444 454	0.196 783 241 692 912	0.949 093 390 834 058 0	1.026 817 877 801 640 0
6	− 0.852 053 333 537 505	0.751 474 209 363 435	− 0.661 765 016 131 294 0	− 0.134 428 104 087 436 0
7	0.956 383 291 469 380	− 0.845 945 944 212 169	1.094 838 134 031 300 0	− 0.064 661 939 780 653 1
8	1.239 472 990 692 190	0.667 568 239 475 322	0.521 379 060 917 113 0	0.237 237 092 227 149 0
9	0.198 526 853 687 727	− 1.565 449 304 932 260	0.013 421 859 051 526 7	− 0.766 714 878 527 624 0

Table 21 Weights of connections between neurons in the hidden and output layer of Model 3

*n*th neuron in the hidden layer	w_{mn} (*m*th neuron in the output layer, $m = 1$)
1	0.580 166 576 256 576
2	− 0.079 503 008 869 124
3	− 0.815 320 777 549 608
4	− 0.302 665 779 360 440
5	1.596 348 970 694 320
6	− 1.606 875 710 016 290
7	2.044 788 822 670 000
8	− 0.946 476 795 650 771
9	− 0.608 922 854 960 592

Table 22 Biases of neurons in the hidden layer of Model 3

*m*th neuron in the output layer	b_m
1	− 0.160 325 631 766 726 0
2	− 0.598 911 360 261 793 0
3	1.486 999 414 597 990 0
4	0.185 683 349 841 928 0
5	− 0.901 629 614 745 261 0
6	0.700 243 302 769 517 0
7	− 0.069 831 122 241 236 7
8	− 0.248 766 565 458 706 0
9	− 0.393 461 772 735 711 0

Table 23 Biases of neurons in the output layer of Model 3

	*m*th neuron in the output layer ($m = 1$)
b_m	− 0.138 460 556 785 922

References

1. Hekner B, Myalski J, Pawlik T et al (2017) Effect of carbon in fabrication Al-SiC nanocomposites for tribological application. Materials 10(6):679. https://doi.org/10.3390/ma10060679
2. Dong Z, Zheng F, Zhu X et al (2017) Characterization of material removal in ultrasonically assisted grinding of SiCp/Al with high volume fraction. Int J Adv Manuf Technol 93(5/8):2827–2839

3. Xiang J, Xie L, Gao F et al (2018) Methodology for dependence-based integrated constitutive modelling: an illustrative application to SiCp/Al composites. Ceram Int 44(10):11765–11777
4. Ozben T, Kilickap E, Cakir O (2008) Investigation of mechanical and machinability properties of SiC particle reinforced Al-MMC. J Mater Process Technol 198(1/3):220–225
5. Kennedy FE, Balbahadur AC, Lashmore DS (1997) The friction and wear of Cu-based silicon carbide particulate metal matrix composites for brake applications. Wear 203:715–721
6. Ravikiran A, Surappa MK (1997) Effect of sliding speed on wear behaviour of A356 Al-30 wt.%SiCp MMC. Wear 206(1/2):33–38
7. Chen J, Gu L, Liu X et al (2018) Combined machining of SiC/Al composites based on blasting erosion arc machining and CNC milling. Int J Adv Manuf Technol 96(1/4):111–121
8. Monaghan JM (1996) The use of a quick-stop test to study the chip formation of a SiC/Al metal matrix composite material and its matrix alloy. Int J Fatigue 18(3):213–217
9. Hocheng H, Yen SB, Ishihara T et al (1997) Fundamental turning characteristics of a tribology-favored graphite/aluminum alloy composite material. Compos A Appl Sci Manuf 28(9/10):883–890
10. Chan KC, Cheung CF, Ramesh MV et al (2001) A theoretical and experimental investigation of surface generation in diamond turning of an Al6061/SiCp metal matrix composite. Int J Mech Sci 43(9):2047–2068
11. Pramanik A, Zhang LC, Arsecularatne JA (2008) Machining of metal matrix composites: effect of ceramic particles on residual stress, surface roughness and chip formation. Int J Mach Tools Manuf 48(15):1613–1625
12. Manna A, Bhattacharyya B (2004) Investigation for optimal parametric combination for achieving better surface finish during turning of Al/SiC-MMC. Int J Adv Manuf Technol 23(9/10):658–665
13. Palanikumar K, Karthikeyan R (2007) Assessment of factors influencing surface roughness on the machining of Al/SiC particulate composites. Mater Des 28(5):1584–1591
14. Przestacki D, Szymanski P, Wojciechowski S (2016) Formation of surface layer in metal matrix composite A359/20SiCP during laser assisted turning. Compos A Appl Sci Manuf 91:370–379
15. Wojciechowski S, Nowakowski Z, Majchrowski R et al (2017) Surface texture formation in precision machining of direct laser deposited tungsten carbide. Adv Manuf 5(3):251–260
16. Kilickap E (2016) Effect of cutting environment and heat treatment on the surface roughness of drilled Al/SiC MMC. Mater Test 58(4):357–361
17. Kilickap E, Cakir O, Aksoy M et al (2005) Study of tool wear and surface roughness in machining of homogenized SiC-p reinforced aluminium metal matrix composite. J Mater Process Technol 164/165:862–867
18. Benardros PG, Vosniakos GC (2002) Prediction of surface roughness in CNC face milling using neural networks and Taguchi's design of experiments. Robot Comput Integrated Manuf 18(5/6):343–354
19. Mahesh G, Muthu S, Devadasan SR (2015) Prediction of surface roughness of end milling operation using genetic algorithm. Int J Adv Manuf Technol 77(1/4):369–381
20. Kilickap E, Huseyinoglu M, Yardimeden (2011) A optimization of drilling parameters on surface roughness in drilling of AISI 1045 using response surface methodology and genetic algorithm. Int J Adv Manuf Technol 52(1/4):79–88
21. Khorasani AM, Yazdi MRS, Safizadeh MS (2011) Tool life prediction in face milling machining of 7075 Al by using artificial neural networks (ANN) and Taguchi design of experiment (DOE). Int J Eng Technol 3(1):30–35
22. Pimenov DY, Hassui A, Wojciechowski S et al (2019) Effect of the relative position of the face milling tool towards the workpiece on machined surface roughness and milling dynamics. Appl Sci 9(5):842. https://doi.org/10.3390/app9050842
23. Bustillo A, Correa M (2012) Using artificial intelligence to predict surface roughness in deep drilling of steel components. J Intell Manuf 23(5):1893–1902
24. Rodríguez JJ, Quintana G, Bustillo A et al (2017) A decision-making tool based on decision trees for roughness prediction in face milling. Int J Comput Integr Manuf 30(9):943–957
25. Çelik YH, Kilickap E, Yardimeden A (2014) Estimate of cutting forces and surface roughness in end milling of glass fiber reinforced plastic composites using fuzzy logic system. Sci Eng Compos Mater 21(3):435–443
26. Lin JT, Bhattacharyya D, Kecman V (2003) Multiple regression and neural networks analyses in composites machining. Compos Sci Technol 63(3/4):539–548
27. Mia M, Królczyk G, Maruda R et al (2019) Intelligent optimization of hard-turning parameters using evolutionary algorithms for smart manufacturing. Materials 12(6):879. https://doi.org/10.3390/ma12060879
28. Bustillo A, Díez-Pastor JF, Quintana G et al (2011) Avoiding neural network fine tuning by using ensemble learning: application to ball-end milling operations. Int J Adv Manuf Technol 57(5/8):521. https://doi.org/10.1007/s00170-011-3300-z
29. Kilickap E, Yardimeden A, Çelik YH (2017) Effect of cutting environment and heat treatment on the surface roughness in milling of Ti-6242S. Appl Sci 7(10):1064. https://doi.org/10.3390/app7101064
30. Manna A, Bhattacharayya B (2003) A study on machinability of Al/SiC-MMC. J Mater Process Technol 140(1/3):711–716
31. Xiang JF, Pang SQ, Xie LJ et al (2018) Investigation of cutting forces, surface integrity, and tool wear when high-speed milling of high-volume fraction SiCp/Al6063 composites in PCD tooling. Int J Adv Manuf Technol 98:1237–1251
32. Yuan ZJ, Geng L, Dong S (1993) Ultraprecision machining of SiCw/Al composites. CIRP Ann 42(1):107–109
33. Sahoo AK, Pradhan S (2013) Modeling and optimization of Al/SiCp MMC machining using Taguchi approach. Measurement 46(9):3064–3072
34. Khorasani AM, Yazdi MRS, Safizadeh MS (2011) Tool life prediction in face milling machining of 7075 Al by using artificial neural networks (ANN) and Taguchi design of experiment (DOE). Int J Eng Technol 3(1):30–35
35. Gologlu C, Sakarya N (2008) The effects of cutter path strategies on surface roughness of pocket milling of 1.2738 steel based on Taguchi method. J Mater Process Technol 206(1/3):7–15
36. YalcinU Karaoglan AD, Korkut I (2013) Optimization of cutting parameters in face milling with neural networks and Taguchi based on cutting force, surface roughness and temperatures. Int J Prod Res 51(11):3404–3414
37. El-Gallab M, Sklad M (1998) Machining of Al/SiC particulate metal-matrix composites: part I:tool performance. J Mater Process Technol 83(1/3):151–158
38. Grzenda M, Bustillo A, Zawistowski P (2012) A soft computing system using intelligent imputation strategies for roughness prediction in deep drilling. J Intell Manuf 23(5):1733–1743
39. Pala M, Caglar N, Elmas M et al (2008) Dynamic soil-structure interaction analysis of buildings by neural networks. Constr Build Mater 22(3):330–342
40. Hagan MT, Demuth HB, Beale MH (1996) Neural network design. PWS Pub. Co., Boston, p 3632
41. Hagan MT, Menhaj MB (1994) Training feed forward networks with the Marquardt algorithm. IEEE Trans Neural Netw 5(6):989–993
42. MacKay David JC (1991) Bayesian interpolation. Neural Comput 4(3):415–447

43. Bustillo A, Grzenda M, Macukow B (2016) Interpreting tree-based prediction models and their data in machining processes. Integr Comput Aided Eng 23(4):349–367
44. Karabulut Ş (2015) Optimization of surface roughness and cutting force during AA7039/Al_2O_3 metal matrix composites milling using neural networks and Taguchi method. Measurement 66:139–149

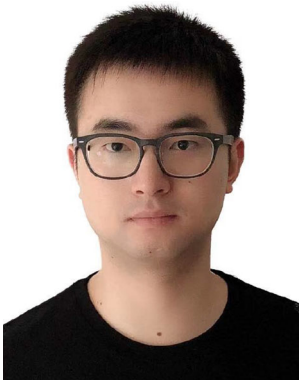

Guo Zhou received his BS and MS degree in Huazhong University of science & technology and Melbourne University, respectively. He currently is a PhD candidate in Tsinghua-Berkeley Shenzhen Institute, Tsinghua University. His research topic is applying the machine learning technologies on the precision manufacturing.

Chao Xu received his PhD from Department of Mechanical Engineering, Tsinghua University, Beijing, China in 2015. He is a research assistant in the Division of Advanced Manufacturing, Shenzhen International School, Tsinghua University. Dr. Xu has shown great interest in vibration monitoring and control of manufacturing systems, ultrasonic-assisted machining processing, et al. He has published more than 30 journal or conference papers.

Yuan Ma received his PhD degree in engineering science from the Department of Mechanical Engineering of Tsinghua University where he was engaged in research in the field of high precision machining technology. At present, he is working in the Laboratory of Intelligent Manufacturing and Precision Machining, and studying advanced machining equipment and technology.

Xiao-Hao Wang received his PhD degree in engineering science from the Department of Precision Instruments and Mechanology of Tsinghua University where he was engaged in research in the field of microfluidics and microfluidic MEMS devices. At present, he is working in the Micro and Nano Technology Research Center, and studying microactuators and their application.

Ping-Fa Feng received his B.S. and M.S. degree from Tsinghua University, China, and received his Ph.D. degree from Technical University Berlin, Germany. He is now a professor in Department of Mechanical Engineering of Tsinghua University, and the director of Division of Advanced Manufacturing, Graduate School at Shenzhen, Tsinghua University. His research interests include high Speed and high performance machining technology, rotary ultrasonic precision machining technology, performance analysis and optimization of manufacturing equipment, on-machine verification technology for NC machining accuracy.

Min Zhang received the Ph.D. degree in mechanical engineering from Dalian University of Technology, China in 2006. He then worked as a postdoctoral researcher in Tsinghua University, China and The University of Minnesota, USA from 2006 to 2011. In 2012, he joined the Faculty at Tsinghua University, Shenzhen, China, where he is currently an Associate Professor with the Graduate School at Shenzhen. He is directing the Microsensors and Actuators Lab. He currently serves as an Editorial Board Member for Advances in Mechanical Engineering.